Dam Break Wave of Thixotropic Fluid

H. Chanson[1]; S. Jarny[2]; and P. Coussot[3]

Abstract: Thixotropy is the characteristic of a fluid to form a gelled structure over time when it is not subjected to shearing, and to liquefy when agitated. Thixotropic fluids are commonly used in the construction industry (e.g., liquid concrete and drilling fluids), and related applications include some forms of mud flows and debris flows. This paper describes a basic study of dam break wave with thixotropic fluid. Theoretical considerations were developed based upon a kinematic wave approximation of the Saint-Venant equations down a prismatic sloping channel. A very simple thixotropic model, which predicts the basic rheological trends of such fluids, was used. It describes the instantaneous state of fluid structure by a single parameter. The analytical solution of the basic flow motion and rheology equations predicts three basic flow regimes depending upon the fluid properties and flow conditions, including the initial "degree of jamming" of the fluid (related to its time of restructuration at rest). These findings were successfully compared with systematic bentonite suspension experiments. The present work is the first theoretical analysis combining the basic principles of unsteady flow motion with a thixotropic fluid model and systematic laboratory experiments.

DOI: 10.1061/(ASCE)0733-9429(2006)132:3(280)

CE Database subject headings: Dam failure; Debris; Bentonite; Industrial wastes; Wastewater.

Introduction

Thixotropic fluids are commonly used in the construction industry for drilling and tunneling: e.g., liquid cements, drilling fluids, and muds (Besq 2000). Other industrial applications include liquid concrete, some paints, the food industry (e.g., liquid dairy products), and clay-water mixtures used by the beauty industry for skin treatment. Related applications encompass some forms of mud flows and debris flows, pasty sewage sludges, and some wastewater treatment residues (e.g., Tabuteau et al. 2004). Thixotropy is the characteristic of a fluid to form a gelled structure over time when it is not subjected to shearing and to liquefy when agitated. Typically, a thixotropic fluid appears as a non-Newtonian fluid exhibiting an apparent yield stress and an apparent viscosity that are functions of both the shear intensity and the current state(s) of structure of the material, sometimes also called "degree(s) of jamming" of the fluid. Under constant shear rate, the apparent viscosity of a thixotropic fluid changes with time until reaching equilibrium. In other words, such fluids exhibit a reversible time-dependent decrease in apparent viscosity under shear rate and a gradual recovery (restructuration) when the shear stress is removed.

In natural mudflows, the interstitial fluid made of clay and water plays a major role on the rheological behavior of the complete material. Since clay-water suspensions have often been considered as thixotropic yield stress fluids, it is likely that thixotropy plays a role in some cases of natural events. However, so far, this is essentially the yielding character of the rheological behavior of these fluids which has been taken into account for modeling either steady (Coussot 1994), slow spreading (Liu and Mei 1989; Balmforth and Craster 1999; Mei and Yuhi 2001), and rapid transient (Laigle and Coussot 1997) free surface flows. There is thus a need to explore the interplay of the yielding and thixotropic characters of such fluids.

This article describes a basic study of dam break wave with thixotropic fluid. Such a highly unsteady flow motion has not been studied to date with thixotropic fluid, despite its practical applications: e.g., mudflow release and testing techniques for superflowing concrete. The results will show that the thixotropic nature of the fluid has a strong influence on the flow motion, while the fluid properties are closely linked with the instantaneous flow conditions. Herein, a theoretical analysis is developed. One-dimensional equations are developed yielding analytical solutions of the problem, and results are discussed. New experimental works are presented, and quantitative results are detailed. It is the purpose of this paper to fill a void in this field, to compare theoretical developments with physical modeling results, and to present new compelling conclusions regarding highly unsteady flow motion of thixotropic fluids.

Fluid Rheology

For a Newtonian fluid, the shear stress acting in a direction is proportional to the velocity gradient in the normal direction. In a laminar flow, Newton's law of viscosity postulates that, for the straight parallel motion of a given fluid, the tangential stress between two adjacent layers of fluid equals:

[1]Dept. of Civil Engineering, The Univ. of Queensland, Brisbane QLD 4072, Australia.

[2]Laboratory of Materials and Structures in Civil Engineering LMSGC, 2 Allée Kepler, 77420 Champs sur Marne, France.

[3]Laboratory of Materials and Structures in Civil Engineering LMSGC, 2 Allée Kepler, 77420 Champs sur Marne, France.

Note. Discussion open until August 1, 2006. Separate discussions must be submitted for individual papers. To extend the closing date by one month, a written request must be filed with the ASCE Managing Editor. The manuscript for this paper was submitted for review and possible publication on September 17, 2004; approved on February 11, 2005. This paper is part of the ***Journal of Hydraulic Engineering***, Vol. 132, No. 3, March 1, 2006. ©ASCE, ISSN 0733-9429/2006/3-280–293/ $25.00.

$$\tau = \mu_f \times \frac{\partial V}{\partial y} \tag{1}$$

where τ=shear stress; μ_f=dynamic viscosity of the fluid; V=velocity; and y=direction perpendicular to the fluid motion. A wide range of non-Newtonian fluids is characterized by some yield stress. In that case, the constitutive law of the fluid motion is often expressed in the form:

$$\tau = \tau_c + \mathsf{F}_1\left(\frac{\partial V}{\partial y}\right) \quad \text{for } \tau > \tau_c \tag{2}$$

where τ_c=constant called yield stress; and F_1=increasing function of the shear rate $\partial V/\partial y$. The Bingham plastic model (i.e., $\mathsf{F}_1 \propto \partial V/\partial y$) appears to be well suited to some sediment-laden flows with large concentrations of fine particles (e.g., Wan and Wang 1994; Julien 1995). A more advanced rheological model is the Herschel–Bulkley fluid model for which $\mathsf{F}_1 \propto (\partial V/\partial y)^m$, where $0 < m \leq 1$ (e.g., Huang and Garcia 1998; Wilson and Burgess 1998).

Various models have been proposed to describe the behavior of thixotropic fluids (e.g., Mewis 1979; Usui 1995; Toorman 1997). Most have a similar structure consisting of an equation of the form (2) now with parameters depending upon some structure parameter(s), associated with some kinetic equation(s) giving the time evolution of the(se) structure parameter(s) as function(s) of time and shear rate. Coussot et al. (2002a) proposed a very simple model which relies upon the same basic ingredients but only expresses the apparent viscosity of the fluid as a function of a single structure parameter λ:

$$\mu = \mu_o \times (1 + \lambda^n) \tag{3}$$

$$\frac{\partial \lambda}{\partial t} = \frac{1}{\theta} - \alpha \times \frac{\partial V}{\partial y} \times \lambda \tag{4}$$

where μ_o, n, θ, and α=four constant parameters for a given fluid; and μ=apparent viscosity of the thixotropic fluid defined as:

$$\mu = \frac{\tau}{\partial V/\partial y} \tag{5}$$

with τ being the shear stress. Eqs. (3) and (4) assume that the degree of jamming of a thixotropic fluid can be represented by a single parameter λ describing the instantaneous state of fluid structure. The latter characterizes the degree of material restructuration and it could represent the degree of flocculation of clays, a measure of free energy landscape for glasses or the fraction of particles in potential wells for colloidal suspensions (Coussot et al. 2002a). One advantage of this model is that flow simulations do not require the determination of a solid-liquid limit, like other yield stress models. This model appeared capable to predict qualitatively the trends of thixotropic fluids, as well as quantitative properties under steady and unsteady states in different flow situations (Ferroir et al. 2004; Roussel et al. 2004).

Discussion

From Eqs. (3) and (4), the apparent viscosity μ is a function of the rate of change of the degree of jamming $\partial\lambda/\partial t$ and of the initial conditions: e.g., the initial degree of jamming $\lambda_o = \lambda(t=0)$. For a constant shear stress τ, the variations in viscosity are driven by the relative values of the two terms of the right-hand side of Eq. (4). For $n > 1$, the viscosity tends either to infinity or to a small asymptotic value μ_o, depending upon the shear stress τ being larger or smaller than a critical value τ_c defined as

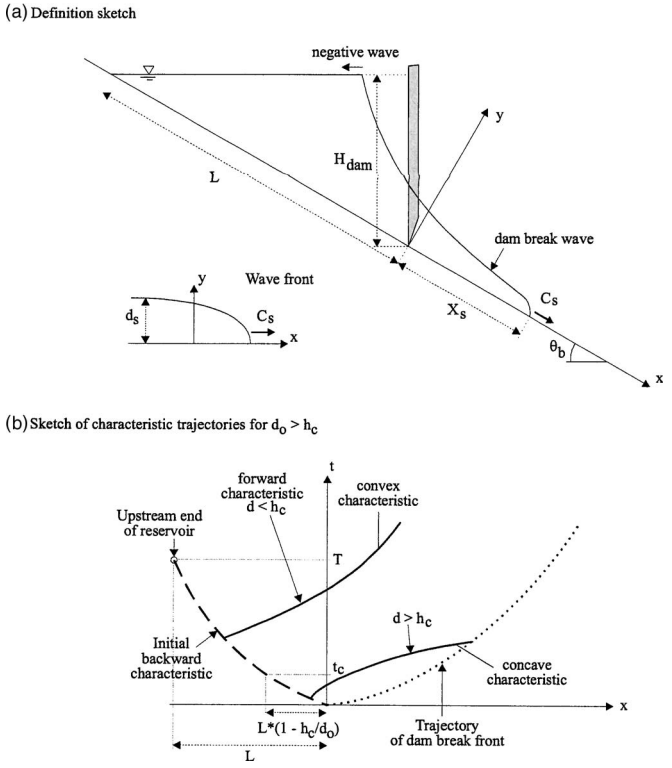

Fig. 1. Dam break wave of thixotropic down a sloping channel: (a) definition sketch; and (b) sketch of characteristic trajectories for $d_o > h_c$

$$\tau_c = \frac{\mu_o \times (1 + \lambda_o^n)}{\alpha \times \lambda_o \times \theta} \tag{6}$$

where λ_o=initial degree of jamming. Thus, although the model of Coussot et al. (2002a) did not explicitly introduce a yield stress, the critical shear stress τ_c [Eq. (6)] may be seen as an apparent yield stress. In particular, its increase with the time of rest (leading to an increase of λ_o) agrees with current observations of yielding of thixotropic pastes (e.g., Alderman et al. 1991).

Theoretical Model

A dam break wave is the flow resulting from a sudden release of a mass of fluid in a channel [Fig. 1(a)]. Hunt (1982, 1984) developed a complete solution of the Saint–Venant equations for a dam break wave down a wide rectangular sloping channel. His development is based upon the kinematic wave approximation which assumes negligible acceleration and inertial terms, and the free surface to be parallel to the channel invert. In these conditions, the Saint-Venant equations become:

$$\text{Continuity equation } \frac{\partial d}{\partial t} + \frac{\partial (V \times d)}{\partial x} = 0 \tag{7}$$

$$\text{Kinematic wave equation } V = \sqrt{\frac{8 \times g}{f}} \times \sqrt{\frac{D_H}{4} \times \sin\theta_b} \tag{8}$$

where d=flow depth or fluid thickness measured normal to the invert; V=depth-average velocity; t=time; x=coordinate in the flow direction positive downstream; f=Darcy friction factor, D_H=hydraulic diameter, and θ_b=angle of the bed with the horizontal [Fig. 1(a)] Eqs. (7) and (8) are valid for both laminar and turbulent flows. For a wide rectangular channel (i.e., $D_H/4=d$), the combination of continuity and momentum equations may be rewritten as:

$$\frac{Dd}{Dt} = 0 \tag{9}$$

along the characteristic trajectory:

$$\text{Forward characteristic trajectory } \frac{dx}{dt} = \frac{3}{2} \times \sqrt{\frac{8 \times g}{f} \times S_o \times d} \tag{10}$$

where D/Dt characterizes the absolute differentiation operator; and $S_o=\sin\theta_b$. Typical characteristic trajectories are shown in Fig. 1(b). At any time, t, the dam break wave profile must further satisfy the conservation of mass:

$$\int_{x=-L}^{X_s} d \times dx = \frac{1}{2} \times H_{\text{dam}} \times L \times \cos\theta_b = \frac{1}{2} \times d_o \times L \tag{11}$$

where L=reservoir length; H_{dam}=dam height; d_o=initial reservoir height measured normal to the chute invert; and X_s=wave front position (Fig. 1).

The dam removal is associated with the dam break wave propagation, as well as a backward characteristic propagating upstream into the reservoir initially at rest (Fig. 1). Since the propagation of the initial negative (backward) wave is relatively rapid, the kinematic wave approximation is improper and the complete equations of Saint Venant must be solved. The initial backward characteristic propagates in a fluid at rest ($V=0$, $S_f=0$) in a triangular reservoir. Its trajectory is

$$\text{Initial backward characteristic } \frac{dx}{dt} = -\sqrt{g \times d} \tag{12}$$

where the water depth d=linear function of the distance x from the gate for a triangular reservoir as sketched in Fig. 1. After rearranging and integrating Eq. (12), it yields the upstream extent of the negative wave:

$$\text{Initial backward characteristic } x = -\frac{1}{4} \times g \times S_o \times t^2 \tag{13}$$

where t=time from dam removal. From Eq. (13), we deduce that, for a two-dimensional triangular reservoir, the initial backward characteristic reaches the reservoir upstream end at

$$T = \sqrt{\frac{4 \times L}{g \times S_o}} \tag{14}$$

and T is shown in Fig. 1(b).

Application to Thixotropic Fluids

For the model of Coussot et al. (2002a), the rheological equations of the thixotropic fluid may be approximated by assuming:

$$\tau_o \approx \mu \times \frac{V}{d} \tag{15}$$

$$\frac{\partial V}{\partial y} \approx \frac{V}{d} \tag{16}$$

where τ_o=boundary shear stress; and μ=apparent fluid viscosity. Eqs. (15) and (16) are one-dimensional approximations. With these, the kinematic wave approximation ($S_o=S_f$) yields:

$$\text{Kinematic wave approximation } V = \frac{\rho \times g \times S_o \times d^2}{\mu_o \times (1+\lambda^n)} \tag{17}$$

since the Darcy friction factor f is defined as:

$$f = \frac{8 \times \tau_o}{\rho \times V^2} \approx \frac{8 \times \mu}{\rho \times V \times d} = \frac{8 \times \mu_o \times (1+\lambda^n)}{\rho \times V \times d} \tag{18}$$

Combining Equations (10), (17), and (18), the equation of the forward characteristic trajectory becomes:

$$\text{Forward characteristic trajectory } \frac{dx}{dt} = \frac{3}{2} \times \frac{\rho \times g \times S_o \times d}{\mu_o \times (1+\lambda^n)} \tag{19}$$

Along a characteristic trajectory, the degree of jamming of the material satisfies:

$$\frac{d\lambda}{dt} = \frac{1}{\theta} - \alpha \times \frac{\rho \times g \times d \times S_o}{\mu_o} \times \frac{\lambda}{1+\lambda^n} \tag{20}$$

with d=constant along the forward characteristic [Eq. (9)]. The trajectory is not a straight line since λ is a function of time and space [e.g., Fig. 1(b)].

Discussion

Several analytical developments may be derived in particular cases including for $\theta \to +\infty$ or for integer values of n (Chanson et al. 2004). More generally, for $n>1$, Eq. (20) predicts different behaviors along a forward characteristic depending upon the sign of $d\lambda/dt$ and the initial degree of jamming $\lambda(t=0)=\lambda_o$. It may be rewritten as

$$\frac{d\lambda}{dt} = \mathsf{F}_2(\lambda) \tag{21}$$

Note that the function $\lambda/(1+\lambda^n)$ tends to zero for $\lambda \to 0$ and $\lambda \to +\infty$, and it has a maximum for $\lambda=\lambda_c=(n-1)^{-1/n}$. Hence, the equation $\mathsf{F}_2(\lambda)=0$ has zero real solution, one solution λ_c or two solutions λ_1 and λ_2 depending upon the value of the dimensionless viscosity:

$$\frac{\mu_o}{\theta \times \alpha \times \rho \times g \times d \times S_o}$$

The function $\mathsf{F}_2(\lambda)$ (i.e., $d\lambda/dt$) is positive for $\lambda \to 0$ and $\lambda \to +\infty$. It is negative for $\lambda_1<\lambda<\lambda_2$ when the equation $\mathsf{F}_2(\lambda)=0$ has two real solutions.

For a dam break down a sloping channel, Eq. (20) gives at the time origin ($t=0$):

Table 1. Summary of Possible Flow Situations along a Forward Characteristic

Condition	λ	$\frac{d\lambda}{dt}$	Forward characteristics	Remarks
(1) $\frac{\mu_o}{\theta\times\alpha\times\rho\times g\times d\times S_o}>\left(\frac{1}{n-1}\right)^{1/n}$	$\to-\infty$ for $t\to+\infty$	>0 for $t\geq 0$	Series of convex curves	Evolution toward complete stoppage.
(2) $\frac{\mu_o}{\theta\times\alpha\times\rho\times g\times d\times S_o}<\left(\frac{1}{n-1}\right)^{1/n}$				
(3.1) $\lambda_o>\lambda_2$	$\to+\infty$ for $t\to+\infty$	>0 for $t\geq 0$ $\to 1/\theta$ for $t\to+\infty$	Series of convex curves	Evolution toward complete stoppage.
(3.2) $\lambda_1<\lambda_o<\lambda_2$	$\to\lambda_1$ for $t\to+\infty$	≤ 0 for $t\geq 0$ $\to 0$ for $t\to+\infty$	Series of concave curves tending to straight lines	Evolution toward constant viscosity fluid.
(3.3) $\lambda_1<\lambda_o$	$\to\lambda_1$ for $t\to+\infty$	≥ 0 for $t\geq 0$ $\to 0$ for $t\to+\infty$	Series of convex curves tending to straight lines	Evolution toward constant viscosity fluid.

Note: λ_1,λ_2=Solutions of the equation $F_2(\lambda)=0$ with $\lambda_1<\lambda_c<\lambda_2$.

$$\left(\frac{d\lambda}{dt}\right)_{t=0}=\alpha\times\frac{\rho\times g\times d\times S_o}{\mu_o}\times\left(\frac{\mu_o}{\theta\times\alpha\times\rho\times g\times d\times S_o}-\frac{\lambda_o}{1+\lambda_o^n}\right) \tag{22}$$

along the forward characteristic where d=constant and λ_o=initial degree of fluid jamming. For

$$\frac{\mu_o}{\theta\times\alpha\times\rho\times g\times d\times S_o}>\left(\frac{1}{n-1}\right)^{1/n} \quad \text{(Case 1)}$$

$d\lambda/dt$ is positive initially and $\lambda(t>0)>\lambda_o$. By extension, $d\lambda/dt$ is positive everywhere along the characteristic trajectory for $t\geq 0$. That is, λ increases monotically toward the wave front. For large times ($t\gg 1$), $d\lambda/dt$ tends to $1/\theta$ and the degree of jamming λ tends to an infinite value: i.e., complete stoppage. Note that the result is independent of the initial degree of jamming λ_o.

A similar reasoning may be developed for:

$$\frac{\mu_o}{\theta\times\alpha\times\rho\times g\times d\times S_o}<\left(\frac{1}{n-1}\right)^{1/n} \quad \text{(Case 2)}$$

with three basic flow situations depending upon the signs of $(\lambda_o-\lambda_1)$ and $(\lambda_o-\lambda_2)$, where λ_1 and λ_2 are the solutions of the equation $F_2(\lambda)=0$ with $\lambda_1<\lambda_2$. All the trends are summarized in Table 1.

Remarks

An intermediate case occurs for

$$\frac{\mu_o}{\theta\times\alpha\times\rho\times g\times d\times S_o}=\left(\frac{1}{n-1}\right)^{1/n} \quad \text{(Case 3)}$$

Two basic flow situations may take place depending upon the sign of $(\lambda_o-\lambda_c)$. For $\lambda_o>\lambda_c$, the fluid flow tends to complete stoppage and the forward characteristics form a series of convex curves. For $\lambda_o<\lambda_c$, the degree of jamming tends asymptotically to $\lambda=\lambda_c$ for large times, and the fluid flow tends to a constant viscosity fluid behavior $[\mu\to\mu_o\times(1+\lambda_c^n)]$ for large times t. In the (x,t) plane, the forward characteristics form a series of convex curves which tend to straight lines for large times t.

In Table 1, simple dimensional considerations yield a characteristic length scale h_c defined as:

$$h_c=\frac{\mu_o\times(n-1)^{1/n}}{\theta\times\alpha\times\rho\times g\times S_o} \tag{23}$$

For flow depths smaller than the characteristic flow depth h_c, the "degree of jamming" λ increases monotically along each forward characteristic until fluid stoppage. h_c is somehow a critical fluid thickness below which the fluid flow motion tends to complete stoppage under certain conditions. Dimensional considerations yield further a characteristic time scale t_c defined as

$$t_c=\sqrt{\frac{4\times L}{g\times S_o}\times\left(1-\frac{h_c}{d_o}\right)} \quad \text{for } h_c<d_o \tag{24}$$

Application to a Dam Break Flow

The above discussion was developed along a forward characteristic on which the flow depth d was a constant [Eq. (9)]. It may be extended to the sudden dam break of a finite volume reservoir [Fig. 1(a)]. Considering a series of characteristics issued from the initial negative characteristic, the flow depth d is constant on each forward characteristic and it must satisfy: $0\leq d\leq d_o$, where d_o =initial reservoir thickness at the gate ($x=0$). Three flow situations may occur depending upon the initial degree of fluid jamming λ_o and the ratio d_o/h_c.

Case A

For reservoir depths less than the characteristic fluid thickness (i.e., $d_o<h_c$), $d\lambda/dt$ is positive for $t\geq 0$ on each forward characteristic. The degree of jamming of the fluid increases monotically with time until fluid stoppage. The extent of fluid flow is limited and the flow motion is relatively slow until complete stoppage. The result is independent of the initial degree of fluid jamming λ_o.

Case B

For large initial reservoirs (i.e., $d_o>h_c$), each characteristic may have a different behavior from adjacent characteristics depending upon the signs of $(\lambda_o-\lambda_1)$ and $(\lambda_o-\lambda_2)$. Typical trends are illustrated in Fig. 2, showing time variations of λ and dimensionless effective viscosity along a forward characteristic. Note that the

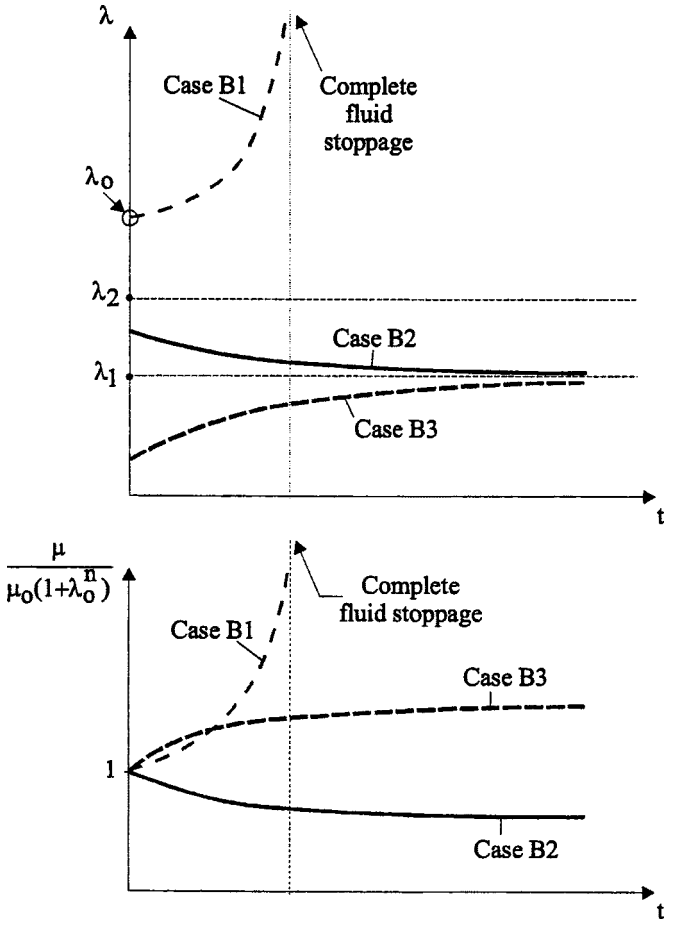

Fig. 2. Variations of the "degree of jamming" and dimensionless effective viscosity with increasing time along forward characteristics in a dam break wave down a sloping channel

solutions λ_1 and λ_2 of Eq. (21) are functions of the flow depth itself. That is, λ_1 increases and λ_2 decreases with decreasing flow depth. At the limit, $\lambda_1=\lambda_2=\lambda_c$ for $d=h_c$.

Following the initial backward characteristic, the flow depth satisfies $h_c<d<d_o$ for $0<t<t_c$ and $0<d<h_c$ for $t_c<t<T$, where T is the time taken by the initial characteristic to reach the reservoir upstream end [Eq. (14)] [Fig. 1(b)]. On each forward characteristic issued from the initial negative characteristic at $t>t_c$, the flow depth d is less than the characteristic fluid thickness h_c. $d\lambda/dt$ is positive everywhere along the forward characteristic and the degree of fluid jamming λ increases monotically until complete stoppage. For $d<h_c$, the flow motion is relatively slow and the extent of fluid flow is limited until complete stoppage.

For $\lambda_o>\lambda_2(d_o)$, $d\lambda/dt$ is positive everywhere along all forward characteristics. λ and μ increases monotically until complete flow stoppage (Case B1) (Fig. 2). The forward characteristics form a series of convex curves in the (x,t) plane. The extent of flow motion is moderate until fluid stoppage.

For $\lambda_1<\lambda_o<\lambda_2(d_o)$ (Case B2), $d\lambda/dt$ is negative along the forward characteristics initially. The fluid flow tends to a constant viscosity behavior $[\mu=\mu_o\times(1+\lambda_1^n)]$ with increasing time toward the wave front (Fig. 2). The characteristics form a series of concave curves which tend to straight lines. That is, the fluid flow tends to a rapid flow motion toward the wave front.

Similarly, for $\lambda_o<\lambda_1(d_o)$ (Case B3), $d\lambda/dt$ is positive initially although it tends to zero with increasing time. On the forward characteristics, the fluid flow tends to a constant viscosity or fast motion $[\mu=\mu_o\times(1+\lambda_1^n)]$ toward the shock. The forward characteristics form a series of convex curves which tend to straight lines for large times.

Basically, Cases B2 and B3 tend to relatively similar flow conditions (Fig. 2). For each forward characteristic issued from the initial backward characteristic at $t<t_c$, the flow depth on the forward characteristics satisfies $d>h_c$. That is, the fluid flow tends to a rapid (low viscosity) flow motion toward the wave front. Along the other forward characteristics issued from the initial backward characteristic at $t>t_c$, the flow depths satisfy $d<h_c$ on these characteristics. The flow motion is relatively slow and the extent of fluid flow is limited until complete stoppage.

Case C

For very large initial reservoirs (i.e., $d_o\gg h_c$) and an initial degree of jamming λ_o such as $\lambda_o\ll\lambda_2(d_o)$, the fluid flows as a quasi-constant viscosity wave motion. The flow might be laminar or turbulent depending upon the flow Reynolds number. In any case, the flow motion is relatively rapid and it will stop only when the fluid thickness becomes less than the characteristic fluid thickness h_c. The maximum extent of the wave front may be deduced from the equation of conservation of mass. Assuming that complete stoppage occurs for $d=h_c$ and that the final fluid thickness remains h_c, the continuity equation [Eq. (12)] yields the final wave front position $(X_s)_{\text{end}}$:

$$(X_s)_{\text{end}}=\frac{1}{2}\times\frac{\theta\times\alpha\times\rho\times g\times S_o\times d_o\times L}{\mu_o\times(n-1)^{1/n}} \tag{25}$$

Eq. (25) is a crude approximation assuming a two-dimensional flow. But its qualitative trends are coherent with both fluid rheological properties and flow motion equations.

Summary

In summary, three flow regimes may be observed depending upon the initial degree of fluid jamming λ_o and of the ratio d_o/h_c. These flow regimes are: (1) A relatively rapid flow stoppage for relatively small mass of fluid ($d_o/h_c<1$) or large initial rest period T_o (i.e., large λ_o) (Cases A and B1); (2) a fast flow motion for large mass of fluid ($d_o/h_c\gg1$) (Case C); and (3) an intermediate motion initially rapid before final fluid stoppage for intermediate mass of fluid ($d_o/h_c>1$) and intermediate initial rest period T_o (i.e., intermediate λ_o) (Cases B2 and B3).

Experimental Facilities

New experiments were performed in the Laboratory of Materials and Structures in Civil Engineering (LMSGC). The facility was a 2 m long, 0.34 m wide, tilting flume. The 0.35 m high sidewalls were made of 12 mm thick 2 m long polycarbonate panels. The floor was a 20 mm thick laminated timber sheet covered with grade 150 sandpaper to minimize slippage. A removable gate, made of polycarbonate, was tilted 15° with the direction normal to the channel invert. All experiments were conducted with a fixed bed slope $\theta_b=15°$ for which the sluice gate was vertical. In addition, some qualitative experiments were conducted on a smaller inclined plate (0.80 m long, 0.48 m wide) covered with sandpaper. Further details were reported in Chanson et al. (2004).

Instrumentation

The channel slope was measured with an electronic inclinometer Digital Protactor Pro360 with an accuracy of 0.1°. For the preparation of the suspensions, the bentonite and water were weighted using a balance Sartorius LP3200D with an accuracy of less than 0.01 g. During experiments, the mass of bentonite suspension was weighted with a balance Metler PM16. The range was 50 g to 16 kg, and the error was less than 1 g. The rheological properties of suspensions were determined with a Rheometer Bohlin Instruments C-VOR 200 NF, equipped with two rough circular disk (⌀=40 mm).

Flow visualizations were performed with four digital video cameras with high-shutter speed: Canon MV500i (25 frames (fr)/s, shutter: Up to 1/8,000 s), Sony CDR-TRV950E 3 charge coupled device CCD (25 fr/s, shutter: Up to 1/10,000 s), Olympus Camedia C700 (15 fr/s, shutter: Up to 1/1,000 s), and a CCD camera (25 fr/s) connected to a computer system.

Free-surface elevations were further measured using the CCD camera at the intersection of a series of laser beams (He/Ne 10 mW) at low incidence with the free surface. The camera recorded 25 frames per second with 256 grey levels at high resolution (1024×1280 pixels). The data were analyzed using a Mourier projection method.

Fluid Preparation

Great care was taken to systematically and consistently prepare the thixotropic fluid using the same procedure, described by Huynh et al. (2001) and Coussot et al. (2002b). Solid mass concentrations of 5 to 20% were used, although most tests were performed with 10, 13, 15, and 17% mass concentration suspensions. The bentonite solution was prepared with distilled water and industrial grade bentonite (Impersol powder, Société Française des Bentonites et Dérivés, France) with no chemical additives. The precision on bentonite mass concentration was less than 0.1%. The bentonite-water suspension was first agitated continuously for about 3 h to ensure complete homogenization. Mixing was performed with a Perrier Labotest GMP Type 32 mixer. The suspension was then left to rest for at least 48 h to allow further hydration and dispersion of bentonite particles. For completeness, the 13% solution was prepared with a 20% solution diluted accordingly with distilled water. The 17% solution was prepared by combining 10% and 20% solutions with the appropriate quantities.

Fluid Properties

Basic properties of Bentonite suspensions were measured with a rheometer equipped with two rough circular disks separated by a 1 mm gap. The gap was selected to be at least ten times the mean particle size. Since some very-fine sand particles were detected, the gap was set at 1 mm. The shear stress and the shear rate in the fluid were approximated with the usual rheometrical formulae neglecting shear rate and shear stress heterogeneities. For each rheological test, a small sample of well-stirred liquid was placed between the plates. The tests were performed under controlled stress for relatively short durations at a constant temperature (25°C). The specimen was presheared at a constant shear rate of 500 s^{-1} for 20 s. It was then rested for a known period T_o before being subjected to a controlled stress loading and unloading of 1 min each.

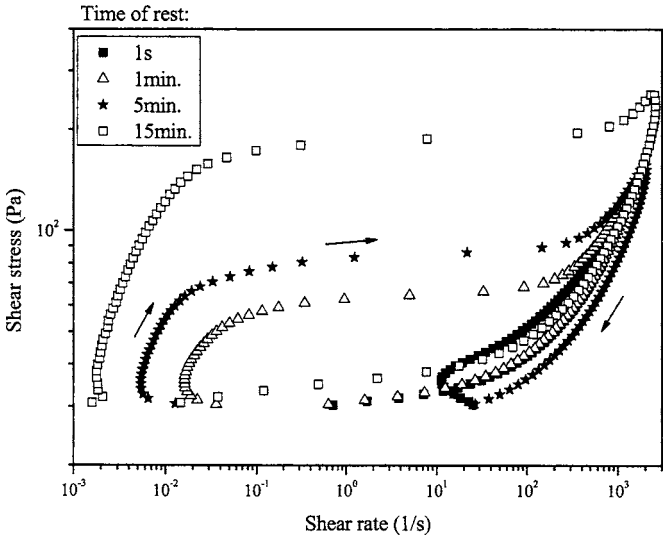

Fig. 3. Rheograms for the bentonite suspension (C_m=0.15) obtained from an increasing-decreasing stress ramp after different times of rest following preshear

The corresponding rheograms τ versus $\partial V/\partial y$ exhibited a stress plateau (rapid increase of shear rate for a small increase in shear stress), the level of which can be considered to reflect the apparent yield stress of the material (e.g., Fig. 3). Results provided some information on the apparent yield stress of the fluid, τ_c, and an effective viscosity μ as functions of the bentonite suspension mass concentration C_m and rest time T_o. Note that a more complete characterization of the rheological behavior of such thixotropic fluids would require the determination of the parameters of a thixotropic model. Such work was carried out successfully for a bentonite suspension (Roussel et al. 2004). Within the frame of the present work, we only proceeded to a more rapid but approximate characterization which already provide some basic information.

Except for the shortest time T_o, after a slow increase in shear rate probably corresponding to the viscoelastic solid regime of the materials, the corresponding rheograms (τ versus $\partial V/\partial y$) associated with the progressive loading exhibited a stress plateau: i.e., a rapid increase in shear rate for a small increase in shear stress (see typical results in Fig. 3). The level of this plateau (τ_{c1}) constitutes the apparent yield stress of the material which increases with T_o (see Table 2), as predicted by the rheological model [Eq. (6)]. Then, the rheograms associated with the unloading have the typical aspect expected for yield stress fluids: While the shear rate tends toward zero, the shear stress progressively decreases toward a finite value (τ_{c2}) which is a kind of critical stress for apparent fluid stoppage. Along this curve (τ versus $\partial V/\partial y$), the material is not too far to have reached steady-state flow conditions since it has rapidly sheared at the highest shear rate reached during the loading phase. The values of τ_{c2} seem indeed mostly independent of the time of rest T_o (Table 2). Both τ_{c1} and τ_{c2} increase with the solid fraction of the material. In the rheological model, these variations of apparent yield stress for start flow and apparent yield stress for flow stoppage as functions of solid fraction and time of rest are reasonably well reproduced by, respectively, an increase in μ_o or an increase in λ_o.

Table 2. Measured Properties of Bentonite Suspensions

		T_o=1 s			T_o=60 s			T_o=300 s			T_o=900 s		
C_m	ρ (kg/m^3)	τ_{c1} loading (Pa)	τ_{c2} unloading (Pa)	μ (Pa s)	τ_{c1} loading (Pa)	τ_{c2} unloading (Pa)	μ (Pa s)	τ_{c1} loading (Pa)	τ_{c2} unloading (Pa)	μ (Pa s)	τ_{c1} loading (Pa)	τ_{c2} unloading (Pa)	μ (Pa s)
0.10	1,064	—	2.7	0.31	11	2.5	0.094	32	2.6	0.456	42	3.4	0.572
0.13	1,085	37	14.8	0.522	50	14	0.555	90	16.2	0.882	165	21.1	0.635
0.15	1,100	45	32.2	0.169	70	33	0.152	90	31	0.062	200	37.3	0.123
0.17	1,115	95	43.3	0.217	105	44.5	0.191	210	55	0.152	300	—	—

Note: τ_c=apparent yield stress; and μ=effective viscosity during unloading phase.

Table 3. Summary of Experimental Flow Conditions with a Constant Slope θ_b=15° in the Large Facility (W=0.34 m)

Mass concentration C_m	Solution density ρ (kg/m^3)	Test No.	Mass M (kg)	Initial height d_o (m)	Rest time T_o (s)	Front end position $(X_s)_{end}$ (m)	End fluid thickness d_{end} (m)	Type of flow	Remarks
0.10	1,063.7	11	1.505	0.0472	300	N/A[a]	0.0010	II	
		10	4.047	0.0774	14,220	N/A	—	I–II	
		9	4.059	0.0776	300	N/A	0.0012	I	
		27	4.149	0.0784	80,880	N/A	—	III to IIIb	Several packets of gelled fluid after first packet.
0.13	1,085.1	25	1.614	0.0484	60	0.643	0.0043	II	
		24	2.728	0.0629	60	1.215	0.0041	II	
		23	3.69	0.0732	60	N/A	0.0039	I	Almost transition between flow Types I and II at downstream end.
		21	3.718	0.0735	2,400	1.204	0.0055	II	Possibly close to transition between flow Types II and III, with slight "crescent of crust croissant" at leading edge.
		22	3.72	0.0735	7,200	1.089	0.0046	III	
		20	3.924	0.0755	62,160	N/A	—	IIIb	Two packets plus one slide. Mass of first two packets: 1.812 kg. Mass of 3rd block (slide): 0.773 kg. Mass reservoir behind 3rd block: 1.339 kg.
		19	3.936	0.0756	900	N/A	0.0036	II	
		18	3.952	0.0758	300	N/A	0.0033	II	
0.15	1,099.8	4	3.141	0.0671	60	0.72	0.0073	II	
		3	3.364	0.0694	60	0.805	—	II	
		2	3.504	0.0709	60	1.007	0.0063	II	
		7	3.652	0.0723	900	0.51	0.008	II to III	
		6	3.686	0.0727	300	0.753	0.083	II	
		8	3.689	0.0727	2400	0.565	—	III	
		5	3.707	0.0729	60	0.958	0.0067	II	
		1	3.786	0.0737	60	1.055	—	II	
		26	3.974	0.0755	62,100	0.042	—	IIIb–IV	Sliding of one block without flow motion.
		26b	3.974	0.0755	62,100	N/A	—	Sliding	At end of Test 26, vibration of plate leading to two-dimensional sliding of 1 block.
0.17	1,115.0	17	3.461	0.0699	20	0.381	—	II	
		15	3.532	0.0707	300	0.241	—	II	
		16	3.579	0.0711	900	0.15	—	III	
		14	3.65	0.0718	60	0.527	—	II	
0.20	1,138.4	13	3.536	0.0700	30	0.078	—	II or III	High-speed mixing of suspension for 3 min before test.
		12	3.684	0.0714	60	0	—	IV	No flow.

Note: C_m=mass concentration defined as the ratio of bentonite mass to bentonite and water mass; d_{end}=average fluid thickness after stoppage (laser grid measurement); d_o=reservoir thickness at the gate; T_o=rest time measured from the start of bentonite suspension pouring into the reservoir/mould; and ρ=bentonite suspension density.

[a]Flow past downstream end of plate.

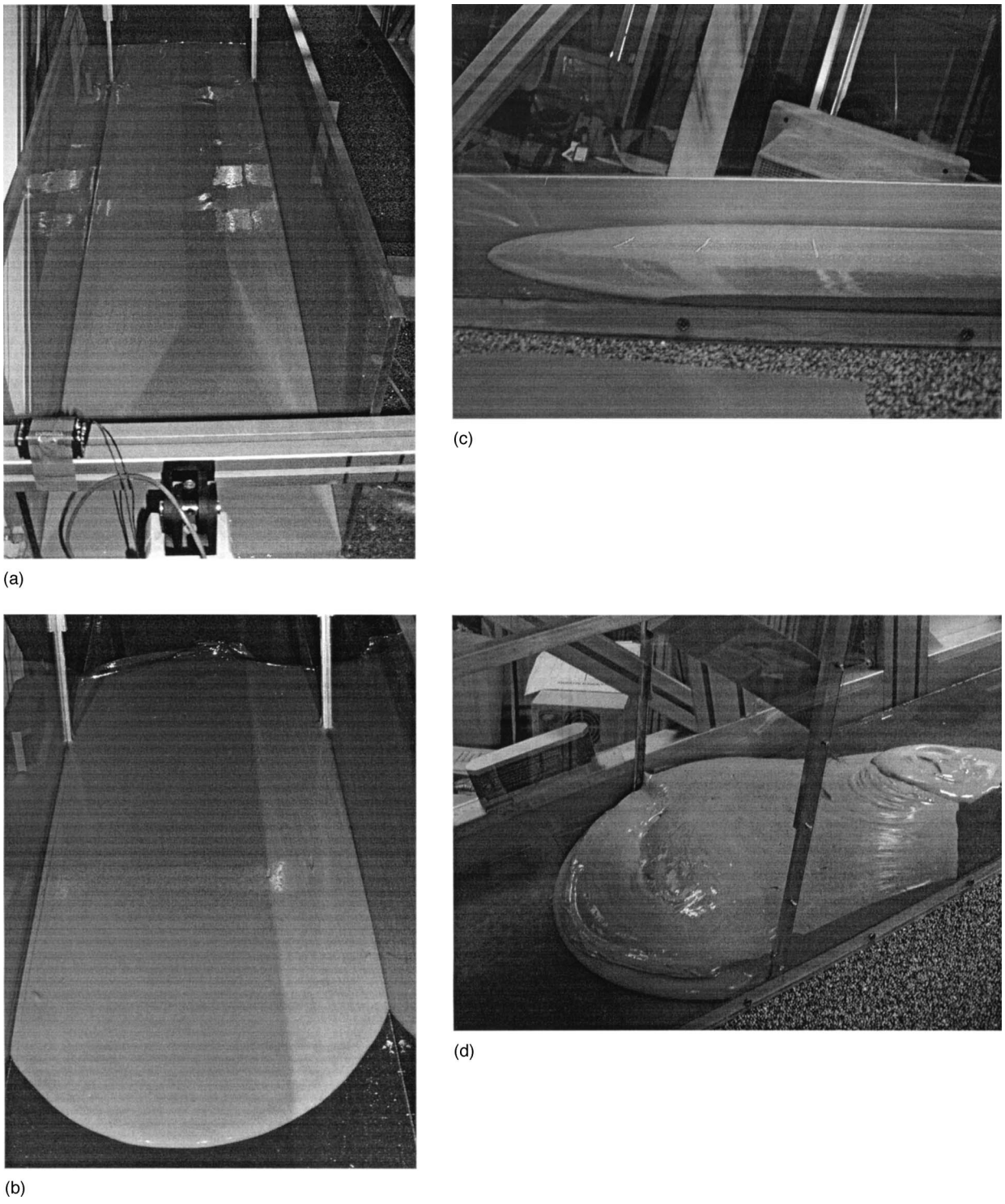

Fig. 4. Photographs of experimental tests: (a) Flow Type I at the end of experiment—the fluid ran past the plate downstream end-Test 23, $\theta_b=15°$, $C_m=0.13$, rest period: $T_o=60$ s; (b) Flow Type II (photograph taken after stoppage); (c) Test 04, $\theta_b=15°$, $C_m=0.15$, rest period: $T_o=60$ s—looking upstream, (b2) Test 05, $\theta_b=15°$, $C_m=0.15$, rest period: $T_o=60$ s—side view—flow direction from right to left; and (d) Flow Type III (photographs taken after stoppage)—Test 16, $\theta_b=15°$, $C_m=0.17$, rest period: $T_o=15$ min. Flow direction from right to left

Preparation of the Experiments

Prior to each test, the bentonite suspension was stirred for about 1 h to ensure that the fluid was destructured completely. Then, the suspension was poured into the reservoir, where it formed a quasi-two-dimensional triangular reservoir. The free surface was quasi-horizontal. The bentonite suspension was then rested for a given period of time T_o before the gate was suddenly opened. The gate removal was rapid (less than 0.1 s). (In the small plate facility, the same procedure was used. The fluid was poured into a mold, and rested for a given period before the mold was suddenly removed.) All measurements were conducted in ambient conditions (i.e., 20°C).

Basic Flow Patterns

Several experiments were conducted systematically on the 15° slope with various masses of fluid, bentonite mass concentrations, and rest times. Details of the experimental flow conditions are summarized in Table 3, which lists the mass of fluid M (Column 4), the initial reservoir fluid thickness d_o at the gate measured normal to the invert (Column 5), the rest period T_o (Column 6), the position of the front at end of experiment (Column 7), measured from the gate, the average fluid thickness after stoppage (Column 8), and the type of flow (Column 9). In Column 7, N/A indicates that the fluid flowed past the downstream end of the channel.

Experimental results demonstrated systematically four basic fluid flow patterns along the 2.0 m long canal. Some examples are illustrated in Fig. 4. For $C_m \leqslant 0.15$ and short relaxation times ($T_o \leqslant 30$ s), the fluid flowed rapidly down the constant slope all along the plate length, and it spilled into the overflow container (Flow Type I) [Fig. 4(a)]. Immediately after gate opening, inertial effects were dominant, leading to some form of jet flow motion, and the flow was basically two dimensional. Afterward, the fluid flowed rapidly down the inclined chute and three-dimensional effects were observed.

For intermediate concentrations and rest periods, the suspension flowed rapidly initially, then decelerated relatively suddenly although it continued to flow slowly for some time before complete stoppage, often upstream of the plate downstream end (Flow Type II) [Fig. 4(b)]. During and after the fluid deceleration, careful video analysis suggested that the front propagation was subjected to some form of perturbations. That is, the wave front (on centerline) seemed to accelerate and decelerate with periods of about 0.1 to 0.25 s (although observations were limited by the video camera frequency of 25 Hz). After stoppage, the fluid had a relatively uniform constant thickness but near the upstream end of the tail [Fig. 4(b)].

For large mass concentrations and long rest periods, the mass of fluid stretched down the slope, until the head separated from the tail [Flow Type III, Fig. 4(b)]. After separation, a thin film of suspension connected the head and tail volumes which could eventually break for long traveling distance of the head. The head had a crescent shape. For long rest periods (i.e., several hours), several successive packets were sometimes observed (Flow Type IIIb). In Flow Type IIIb, the packets of fluid were observed to be about the same mass, while the second and subsequent packets ran slower than the first packet of fluid. Sometimes a last packet would shear from the reservoir fluid although it did not flow (e.g. Test 20). For each packet, the fluid length (in the streamwise direction) measured on the centerline was typically about $1.5 \times d_o$ to $2.5 \times d_o$, independently of mass concentration and rest time. The last flow pattern (Type IV) corresponded to an absence of flow. Sometimes, a slight deformation of the reservoir, with some cracks possibly, were observed.

The experiments showed that the characteristic conditions for the transition between flow regimes were functions of the mass concentration of bentonite suspension C_m, rest time T_o, and initial mass of fluid M. The observations are summarized in Table 3 (Column 9). In other words, the type of flow regime changed from a rapid flow (Type I) to no flow (Type IV, solid structure) with decreasing mass M, increasing mass concentration C_m, and increasing rest period T_o.

For flow conditions near the transition between Flow Types II and III, a thin crescent of re-structured fluid was observed at the surface of the fluid next to the front.

Quantitative Results

The propagation of the wave front was investigated with video cameras and typical results are presented in Fig. 5 showing the dimensionless wave front location X_s/d_o as function of the dimensionless time $t \times \sqrt{g/d_o}$. In addition, the dimensionless wave front celerity $C_s/\sqrt{g \times d_o}$ is plotted (Fig. 5, right vertical axis). Data from several cameras are presented showing good consistency between all data, independently of camera location and type. In addition, a small number of experiments were repeated. The results demonstrated conclusively the repeatibility of the experiments. For Flow Types I and II (possibly some Flow Type III), the extrapolation of present results to an infinitely long inclined plate yields a relationship between wave front location and time with five characteristic periods (before stoppage), and typical results are discussed below.

Flow Motion

The initial instants immediately after gate opening were characterised by a very rapid acceleration of the fluid. The flow was somehow similar to a jet flow motion. The fluid was subjected to an acceleration component parallel to the plate caused by the gravity acceleration component, as well as to an acceleration component normal to the invert as the result of both gravity component and sudden lowering of the reservoir free surface. Neglecting the acceleration component normal to the invert, the wave front location and celerity in the initial instants after gate opening may be deduced from the motion equation as

$$\frac{X_s}{d_o} = \frac{1}{2} \times \left(t \times \sqrt{\frac{g \times \sin\theta_b}{d_o}} \right)^2 \tag{26}$$

$$\frac{C_s}{\sqrt{g \times d_o}} = t \times \sqrt{\frac{g \times \sin\theta_b}{d_o}} \tag{27}$$

assuming little flow resistance. Eqs. (26) and (27) are compared with experimental data in Fig. 6. The comparison is favorable for $t \times \sqrt{g/d_o} < 4.5$ to 6 for which the wave front was two-dimensional. The result demonstrated that the initial flow motion was dominated by inertial effects and bed friction was negligible.

Once the wave front started to become three-dimensional (i.e., to be curved as viewed in elevation), the relationship between front location and time became nearly linear, and the flow motion remained rapid (Fig. 5). For $t \times \sqrt{g/d_o} \sim 10$ to 20, a relatively strong flow deceleration was observed, which was seen by a sharp negative slope of the function $C_s(t)$ (Fig. 5). It is thought that, at the wave front, the fluid motion was characterized by a shear-dominated region next to the invert, an upper fluid layer, and an interfacial zone in between. In the upper flow zone, the fluid was subjected to little stress and it had time to restructure. Its apparent viscosity increased significantly and contributed to greater flow resistance. After the marked flow deceleration, experimental observations showed a relatively slower motion, followed by a very slow flow motion. The latter was nearly a "creeping" motion, until stoppage.

Immediately after gate opening, observations of maximum shock celerity $(C_s)_{\max}$ and corresponding time $t_{\max}$ are summarized in Table 4 (Columns 2 and 3). The results were dependent primarily upon Flow Type (Table 3). A Reynolds number was estimated in terms of the maximum shock celerity $(C_s)_{\max}$, initial reservoir height d_o, and measured fluid properties (Table 1). In

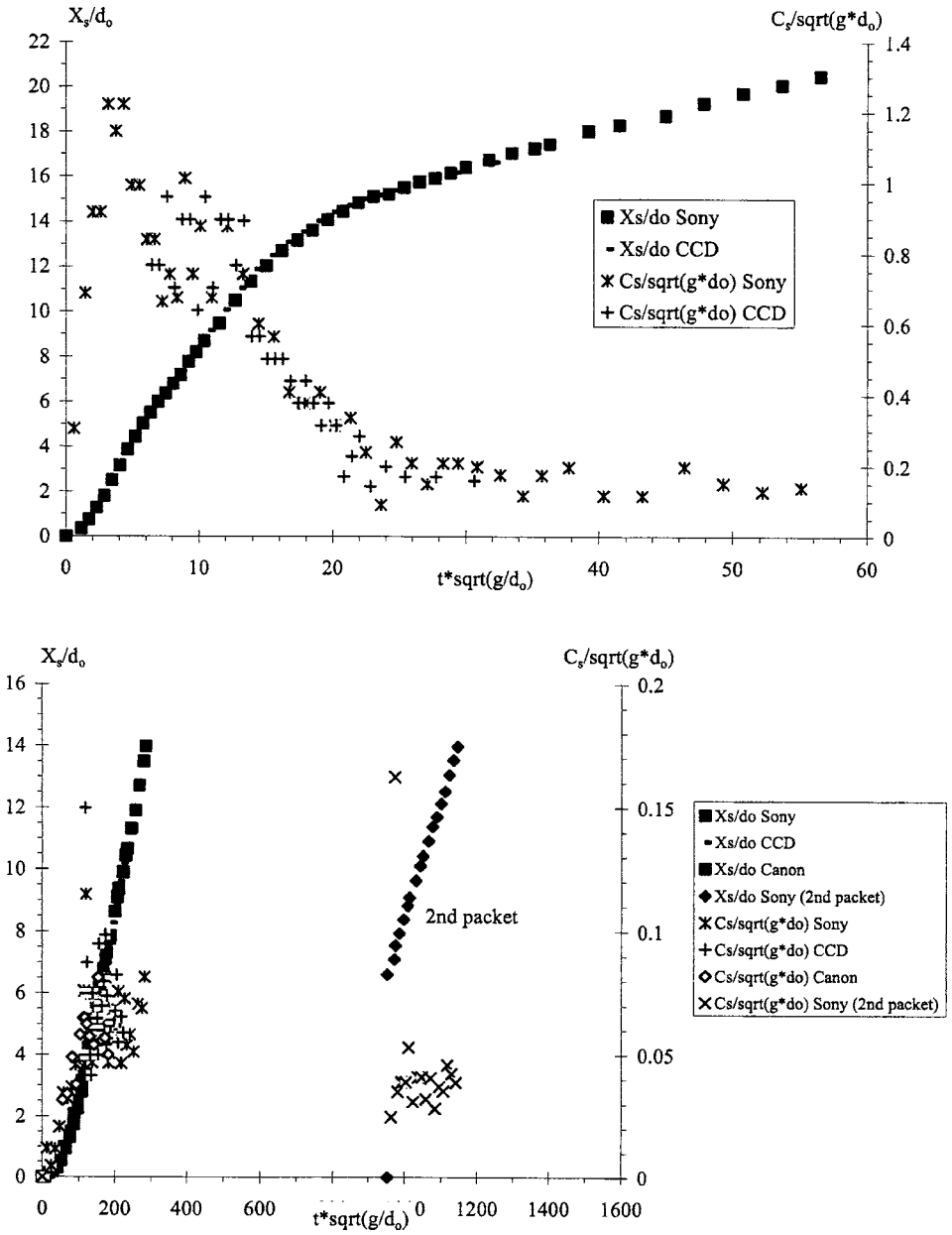

Fig. 5. Wave front propagation on the channel centerline: X_s/d_o as function of the dimensionless time $t\times\sqrt{g/d_o}$: (a) Flow Type II-Test 11, $\theta_b=15°$, $C_m=0.10$, $M=4.0$ kg, rest period: 14,420 s (3 h 57 min); and (b) Flow Type IIIb-Test 20, $\theta_b=15°$, $C_m=0.13$, $M=3.9$ kg, rest period: 62,160 s (17 h 16 min.) Note the data for the second packet of fluid

Flow Type I, the observed Reynolds number ($R\sim310$) was significantly high. Was the flow turbulent? Although the transition between laminar and turbulent flows is typically $R\sim1{,}000$ to 5,000 in industrial circular pipes, this estimate is based upon smooth boundaries. Turbulent flows may be observed for much lower Reynolds numbers with large roughness. In the present study on a rough invert, it cannot be excluded that turbulent flow motion was experienced. The lesser maximum shock celerity observed in Flow Types II and III might indicate some fluid restructuration prior to gate opening.

Front Curvature

During flow motion, the fluid exhibited a curved front, viewed in elevation, for all investigated flow conditions and $t\times\sqrt{g/d_o}>6$. This is well illustrated in Figs. 4(b and c). Typical experimental measurements of wave front shape at several instants after gate opening are presented in Fig. 7. The results showed that the front curvature increased with time, hence the travelled distance X_s from the gate for a given experiment. Further video observations demonstrated slower fluid motion next to the sidewalls.

For all experiments, the flow curvature developed rapidly, and it exhibited a power-law profile that was best fitted by

$$\frac{X}{d_o}\propto\left(\frac{Z}{d_o}\right)^{0.4} \tag{28}$$

where $X=X_s-x$, Z=transverse distance measured from the centerline; x=longitudinal distance from the gate, X_s=coordinate of the

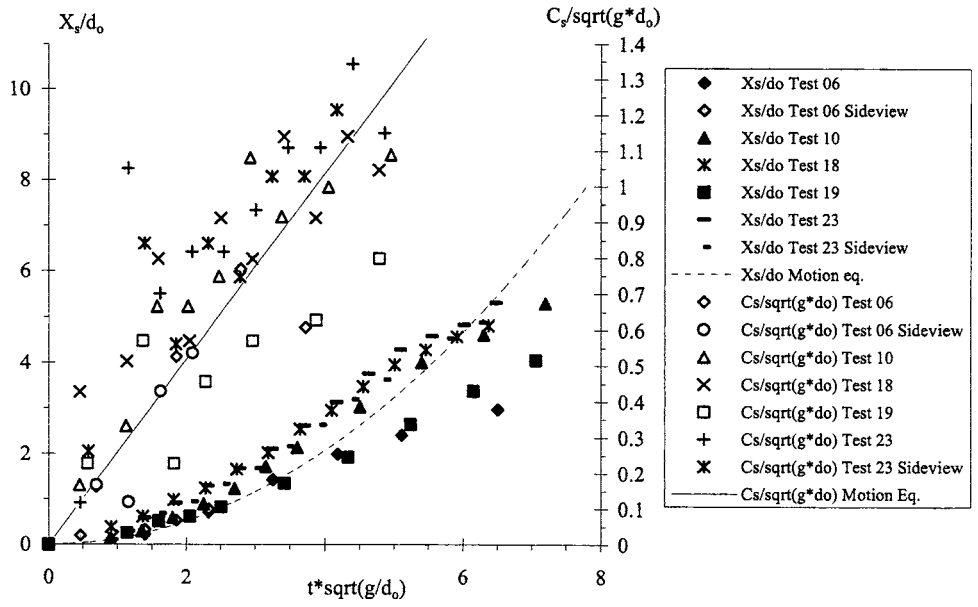

Fig. 6. Wave front propagation immediately after gate opening—comparison with Eqs. (26) and (27)

front; and d_o=initial reservoir thickness at the gate. Basically, $X=0$ and $Z=0$ at the shock front on the channel centerline. Eq. (28) was obtained independently of time t, initial mass M, mass concentration C_m, rest period T_o, and flow regime. It is compared with experimental observations in Fig. 7. Interestingly, Huang and Garcia (1998) presented a photograph showing a similar front curvature with kaolinite suspension mud flows, but they did not elaborate on the shock front curvature.

The front curvature developed rapidly after dam break. Since the polycarbonate panels of sidewalls were very smooth, sidewall friction did not play a preponderant role. Calculations of sidewall boundary layer showed thin shear layers: i.e., typically a few centimeters at $x=0.5$ m. Further shock waves were not experienced. It is hypothesized that the front curvature might be caused by interactions between sidewall and bottom boundary layers. Yet, the marked curvature of surge front over such short distances is not fully understood.

Side Profiles of the Surge Front

Visual observations through the sidewalls showed that the surge front had a smooth shape during the flow motion. A typical example is shown in Fig. 8 during flow motion, where $X=0$ corresponds to the wave front. Test conditions and instantaneous flow properties are given in caption with the time t since gate opening, the wave front position on centerline and at sidewall, and the wave front celerity. Fig. 9 presents the free-surface profile after complete fluid stoppage based upon the deformation of the laser grid illumination.

First, all experimental data demonstrated a smooth shape. In Flow Type III, however, a cap of restructured fluid was observed shortly after gate opening. The finding indicated that the restructured fluid next to the reservoir free surface was not subjected to high shear rate, although it was entrained by the flowing fluid underneath. Second, in Flow Types I and II, the shock front on the centerline was thicker than the nappe of fluid behind. This is illustrated in Figs. 8 and 9 showing a thicker leading edge than the fluid behind. Third, there were consistent differences between the centerline and sidewall profiles. This is seen in Fig. 8.

Observations after fluid stoppage further showed little transverse variations in fluid thickness, and a smooth increase in fluid thickness in the downstream direction towards the shock (Fig. 9). It is proposed that the wave front decelerated first while the fluid

Table 4. Maximum Shock Celerity $(C_s)_{\max}$, Instant $t_{\max}$ at Which It Occurs and Corresponding Flow Reynolds Number $\rho\times(C_s)_{\max}\times d_o/\mu$ (Large Facility)

Flow type	$\frac{(C_s)_{\max}}{\sqrt{g\times d_o}}$	$t_{\max}\times\sqrt{\frac{g}{d_o}}$	$\rho\times\frac{(C_s)_{\max}\times d_o}{\mu}$	Remarks
I	1.5	4.2	310	Three experiments.
II	0.86	3.4	150	13 experiments.
III	0.37	2.3	73	Five experiments.

Note: ρ=fluid density; and μ=measured effective viscosity (Table 2).

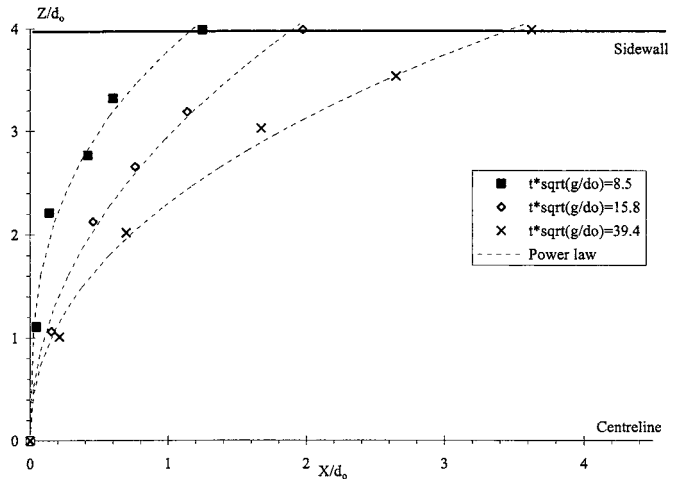

Fig. 7. Curved profiles of the wave front, viewed in elevation of the front. Flow Type I (almost Type II), Test 23, $\theta_b=15°$, $C_m=0.13$, $M=3.7$ kg, rest period: $T_o=60$ s.

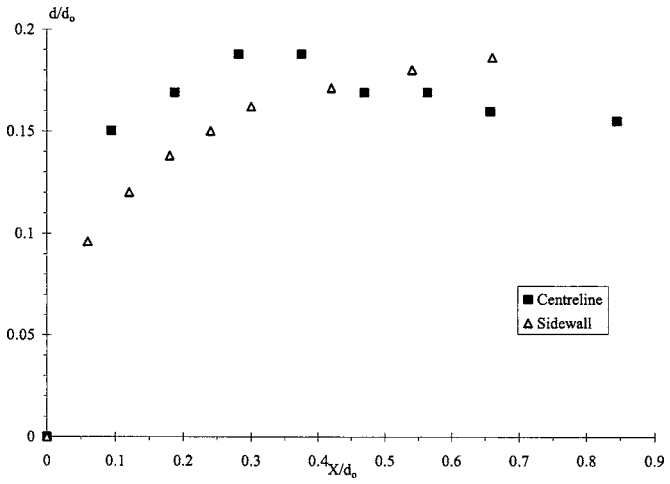

Fig. 8. Longitudinal wave front profile at a fixed time during flow motion (side camera data)—Flow Type I-II—Test 10, $\theta_b=15°$, $C_m=0.10$, $M=4.05$ kg, rest period: $T_o=14{,}220$ s (3 h 57 min.); centerline data: $t=0.91$ s, $X_s=0.575$ m, $C_s=0.56$ m/s; and Sidewall data: $t=1.03$ s, $X_s=0.63$ m, $(X_s)_{\text{wall}}=0.571$ m, $C_s=0.57$ m/s

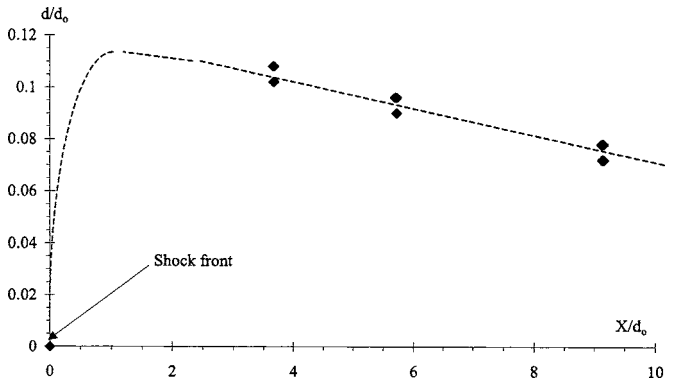

Fig. 9. Longitudinal free-surface profile after complete fluid stoppage (laser grid deformation data: Flow Type II—Test 5, $\theta_b=15°$, $C_m=0.15$, $M=3.71$ kg, rest period: $T_o=60$ s

behind could slow slightly faster, yielding a gradual increase in fluid mass toward the shock. This would be consistent with visual observations showing some tiny fluid motion up to 1 to 2 min after front stoppage.

Discussion: Comparison between Theory and Experiment

The physical observations of flow regimes were in very good qualitative agreement with theoretical considerations, although this has to be further investigated quantitatively. In particular, exactly the same flow regimes were identified as well as same trends for the effects of the bentonite concentration and rest time. For example, theoretical considerations predict an intermediate motion with initially rapid before final fluid stoppage for intermediate mass of fluid M (i.e., $d_o/h_c>1$) and intermediate initial rest period T_o. The theory predicts a faster flow stoppage with increasing rest period. Similarly, it shows that an increase in bentonite mass concentration, associated with an increase in the product $(\theta\times\alpha)$, yields a faster fluid stoppage with a larger final fluid thickness. A similar comparison between theory and physical experiments may be developed for fast-flowing motion and relatively rapid flow stoppage situations. This qualitative agreement between simple theory and reality means that the basic physical ingredients of the rheological model and kinematic wave equations are likely to be at the origin of the observed phenomena. Considering the strongly different flow regimes, involving either solid or liquid regions in a complex interplay, this suggests that—by opposition to usual models devoted to a specific field—a model of this type is capable of reproducing the different stages of flow of natural mass movements which turns from solid to liquid or from liquid to solid. In contrast with the usual separation of materials in distinct categories, the apparent behavior of a jammed material under continuously varying conditions can cover all possible liquid or solid aspects.

Qualitatively and quantitatively, present calculations were in agreement with experimental observations, but for the instants after dam removal (i.e., $t\times\sqrt{g/d_o}<5$). Hunt (1982) showed that, for turbulent flows, the kinematic wave approximation was valid after the wave front travelled approximately four reservoir lengths downstream of the gate: i.e., $X_s/L>4$. The assumption is not valid until the free surface becomes parallel to the chute invert. Hunt (1984) commented however: "*it is possible that an approach similar […] could be used to route the flood downstream and that the result might be valid even for relatively small distance downstream*." With thixotropic fluids, a comparison between experiments and calculations suggested that the kinematic wave approximation seemed reasonable once the wave front traveled approximately one to two reservoir lengths downstream of the gate: i.e., $X_s/L>1$ to 2.

Interestingly, Flow Type III is the only flow pattern not predicted by theoretical considerations. It is believed that this situation simply reflects the limitations of the Saint-Venant equations that are one-dimensional flow equations, and of the kinematic wave approximation that implies a free surface parallel to the chute invert, hence incompatible with the Type III free-surface pattern [e.g. Fig. 4(c)].

Lastly, the gate opening was associated with a negative wave propagation upstream into the reservoir (i.e., drawdown) similar to a reservoir drawdown with laminar and turbulent Newtonian fluids. For most flow conditions, no shearing/sliding was observed in the reservoir tail, but in Flow Type IIIb.

Unusual Flow Patterns and Instabilities

The experimental facility provided an opportunity for additional observations of unusual flow patterns and instabilities. But it must be emphasized that these constituted unusual events that were not representative of the bulk of the experiments.

First, the conditions of fluid preparation were found to be important as discussed by Coussot et al. (2002b). For one experiment, the fluid was not properly destructured initially, and little flow motion was observed. An identical experiment, after careful mixing of the fluid, generated a significantly longer flow rundown. Second, some free-surface anomalies were observed at the end of a few experiments: i.e., after fluid stoppage. These included some spots of fluid restructuration at the surface of Flow Type II after stoppage, or significant free-surface deformations after only a very short fluid motion (Flow Types III and III-IV). Third, in Flow Type IIIb, several successive packets of fluid were observed with a clear "pause" between each motion. Each packet

Fig. 10. Man-made instabilities induced after stoppage, during cleanup in the large facility when the reservoir fluid was pushed over the stopped fluid—Test 05, Flow Type II, $\theta_b=15°$, $C_m=15\%$, $T_o=60$ s, and $M=3.7$ kg. Flow direction from right to left.

could be separated by up to several minutes. In Fig. 5(b), the second packet started 1.5 min after the first packet, and propagated at a slower pace.

Lastly, some form of "roll waves" were seen during the cleanup of fluid after fluid stoppage. Fig. 10 illustrates an example where instabilities developed after pushing the reservoir fluid with a paddle toward the downstream end of chute. Well-defined instabilities were seen when the "pushed" fluid traveled over a thickness of arrested fluid (Fig. 10), but the instabilities disappeared once the it overtook the final wave front position $(X_s)_{\text{end}}$.

Conclusion

In a dam break wave of thixotropic fluid, the interactions between flow motion and fluid rheology are very strong. The fluid is subjected to a continuous transition from a liquid to a solid behaviour at fluid stoppage. Theoretical considerations were developed based upon a kinematic wave approximation of the Saint-Venant equations for a thixotropic fluid flow down a prismatic sloping channel. A simple thixotropic fluid model was used which is based upon a minimum number of parameters, and described the instantaneous state of fluid structure by a single parameter. The analytical solution of the basic flow motion and rheology equations predicted three basic flow regimes depending upon the fluid properties and flow conditions, including the initial degree of jamming of the fluid: (1) a short motion with relatively-rapid flow stoppage for relatively small mass of fluid ($d_o/h_c<1$); (2) a fast flow motion for a large mass of fluid ($d_o/h_c\gg1$); or (3) an intermediate motion initially rapid before final fluid stoppage for intermediate mass of fluid ($d_o/h_c>1$) and intermediate initial rest period T_o. This behaviour, unknown to turbulent or laminar fluid motion, is typical of well-known thixotropic fluid flows, such as pasty cement flows, some mud flows, and subaerial or submarine landslides.

Physical experiments were conducted with bentonite suspensions in a 15° slope channel with a rough invert to avoid slip. For small bentonite mass concentrations C_m and short relaxation times T_o, the fluid flowed rapidly down the slope and spilled into the overflow container (Flow Type I). For intermediate concentrations and rest periods, the suspension initially flowed rapidly, decelerated relatively suddenly, then, continued to flow slowly for sometime before complete stoppage (Flow Type II). For large mass concentrations and long rest periods, the mass of fluid stretched down the slope, until the head separated from the tail (Flow Type III). Sometimes a second and third packet followed (Flow Type IIIb). The last flow pattern (Type IV) corresponded to an absence of flow for large bentonite concentrations and long rest times. Qualitatively, the observations of flow regimes were in good agreement with theoretical considerations. Quantitative informations were documented in terms of wave front location and celerity, wave front curvature, side profile of wave front during, and after flow motion, final fluid thickness, as well as flow motion immediately after gate opening. Some free-surface instabilities are discussed and illustrated.

It is believed that the present study is the first theoretical analysis combining successfully the basic principles of unsteady flow motion (i.e., Saint-Venant equations) with a thixotropic fluid model, as well as the first systematic study of dam break wave of a thixotropic fluid in a large-size facility. It is the belief of the writers that, for such complex systems, this approach combining both rheology and hydraulic engineering is necessary to gain new insights into these complicated flow motions. Further works may include an extension of the theory to three-dimensional flow situations, possibly with some numerical modeling, associated with further physical modeling. Additional experimental works may include high-speed video movies of the flow motion to study wave instabilities during fluid motion, detailed flow measurements of the interactions between sidewall and bottom boundary layers, and a systematic study of peculiar flow instabilities (e.g., Fig. 10).

Acknowledgments

The writers thank Dr. Nicolas Roussel (Division BCC, LCPC Paris) for his valuable comments. They further acknowledge the technical assistance of the LMSGC.

Notation

The following symbols are used in this paper:

A = flow cross-section area (m^2);
C_m = bentonite mass concentration;
C_s = wave front celerity (m/s);
$(C_s)_{\max}$ = maximum shock celerity (m/s);
D_H = hydraulic diameter: $D_H=4\times A/P_W$;
d = flow depth (m) measured normal to the invert;
d_{end} = average fluid thickness (m) measured normal to the chute invert, measured after fluid stoppage;
d_o = initial reservoir height (m) measured normal to the chute invert;
f = Darcy-Weisbach friction factor;
g = gravity constant (m/s^2); $g=9.81$ m/s^2;
H_{dam} = vertical reservoir height (m) at the gate;
h_c = characteristic fluid thickness (m);
L = reservoir length (m);
M = initial mass of fluid (kg)
m,n = exponents;
P_w = wetted perimeter (m);
R = Reynolds number;

S_f = friction slope;
S_o = bed slope: $S_o = \sin\theta_b$;
T = characteristic time (s) when the initial backward characteristic reaches the reservoir upstream end;
T_o = fluid rest time (s);
t = time (s);
t_c = characteristic time (s);
t_{max} = instant (s) at which the shock celerity is maximum: $C_s(t=t_{max})=(C_s)_{max}$;
V = velocity (m/s);
X_s = wave front position (m);
$(X_s)_{end}$ = wave front position (m) at the end of experiment (i.e., after stoppage);
x = longitudinal distance (m) measured from the gate;
y = distance (m) normal to the invert;
Z = transverse distance (m) measured from the centerline;
α = characteristic time of evolution of the fluid structure, assumed constant for a given fluid;
θ = characteristic restructuration time (s);
θ_b = bed slope angle;
λ = degree of jamming of the thixotropic fluid;
λ_c = characteristic degree of jamming of the fluid;
λ_1, λ_2 = characteristic degrees of jamming of the fluid;
λ_o = initial degree of jamming of the fluid;
μ = apparent viscosity (Pa s);
μ_f = fluid dynamic viscosity (Pa s);
μ' = Bingham fluid parameter (Pa s);
μ'' = Herschel–Bulkley fluid parameter (Pa s);
μ_o = characteristic viscosity (Pa s) of destructured thixotropic fluid;
ρ = fluid density (kg/m^3);
τ = shear stress (Pa);
τ_c = 1-yield stress (Pa) and 2-critical shear stress (Pa); and
τ_o = boundary shear stress (Pa).

References

Alderman, N. H., Meeten, G. H., and Sherwood, J. D. (1991). "Vane rheometry of bentonite gels." *J. Non-Newtonian Fluid Mech.*, 29, 291–310.

Balmforth, N. J., and Craster, R. V. (1999). "A consistent thin-layer theory for Bingham plastics." *J. Non-Newtonian Fluid Mech.*, 84, 65–81.

Besq, A. (2000). "Ecoulement laminaire de suspensions de bentonites industrielles. Caractérisation rhéométrique. Ecoulements en conduites axisymmétriques. Applications aux Activités du Génie Civil.." PhD thesis, Univ. of Poitiers, France.

Chanson, H., Coussot, P., Jarny, S., and Tocquer, L. (2004). "A study of dam break wave of thixotropic fluid: Bentonite surges down an inclined plane." *Rep. No. CH54/04*, Dept. of Civil Engineering, The Univ. of Queensland, Brisbane, Australia.

Coussot, P. (1994). "Steady, laminar, flow of concentrated mud suspensions in open channel." *J. Hydraul. Res.*, 32, 535–559.

Coussot, P., Nguyen, A. D., Huynh, H. T., and Bonn, D. (2002a). "Avalanche behavior in yield stress fluids." *Phys. Rev. Lett.*, 88, 175501.

Coussot, P., Nguyen, A. D., Huynh, H. T., and Bonn, D. (2002b). "Viscosity bifurcation in thixotropic yielding fluids." *J. Rheol.*, 46, 573–589.

Ferroir, T., Huynh, H. T., Chateau, X., and Coussot, P. (2004). "Motion of a solid object through pasty (thixotropic) fluid." *Phys. Fluids*, 16(3), 594–601.

Huang, X., and Garcia, M. (1998). "A Herschel–Bulkley model for mud flow down a slope." *J. Fluid Mech.*, 374, 305–333.

Hunt, B. (1982). "Asymptotic solution for dam-break problem." *J. Hydraul. Div., Am. Soc. Civ. Eng.*, 108(1), 115–126.

Hunt, B. (1984). "Perturbation solution for dam-break floods." *J. Hydraul. Eng.*, 110(8), 1058–1071.

Huynh, H. T., Bonn, D., and Coussot, P. (2001). "Caratérisation de la thixotropie de fluides pâteux." ('Thixotropic characteristics of pastes.') *Proc., 36th Colloque Annuel du Groupe Français de Rhéologie GFR*, 72–77.

Julien, P. Y. (1995). *Erosion and sedimentation*, Cambridge University Press, Cambridge, UK.

Laigle, D., and Coussot, P. (1997). "Numerical modeling of mudflows." *J. Hydraul. Eng.*, 123(7), 617–623.

Liu, K. F., and Mei, C. C. (1989). "Slow spreading of a sheet of Bingham fluid on an inclined plane." *J. Fluid Mech.*, 207, 505–529.

Mei, C. C., and Yuhi, M. (2001). "Slow flow of a Bingham fluid in a shallow channel of finite width." *J. Fluid Mech.*, 431, 135–159.

Mewis, J. (1979). "Thixotropy—A general review." *J. Non-Newtonian Fluid Mech.*, 6, 1.

Roussel, N., Le Roy, R., and Coussot, P. (2004). "Thixotropy modeling at local and macroscopic scales." *J. Non-Newtonian Fluid Mech.*, 117(2–3), 85–95.

Tabuteau, H., Baudez, J. C., Bertrand, F., and Coussot, P. (2004). "Mechanical characteristics and origin of wall slip in pasty biosolids." *Rheol. Acta*, 43, 168–174.

Toorman, E. A. (1997). "Modeling the thixotropic behavior of dense cohesive sediment suspensions." *Rheol. Acta*, 36, 56.

Usui, H. (1995). "A thixotropy model for coal-water mixtures." *J. Non-Newtonian Fluid Mech.*, 60, 259.

Wan, Z., and Wang, Z. (1994). "Hyperconcentrated flow." *IAHR Monograph*, Balkema, Rotterdam, The Netherlands.

Wilson, S. D. R., and Burgess, S. L. (1998). "The steady, spreading flow of a rivulat of mud." *J. Non-Newtonian Fluid Mech.*, 79, 77–85.